Available online at www.sciencedirect.com
ScienceDirect
Journal of Hazardous Materials 147 (2007) 120–132
Journal of Hazardous Materials
www.elsevier.com/locate/jhazmat

Methylene blue adsorption by algal biomass based materials: Biosorbents characterization and process behaviour

Vítor J.P. Vilar, Cidália M.S. Botelho, Rui A.R. Boaventura *

LSRE-Laboratory of Separation and Reaction Engineering, Departamento de Engenharia Química, Faculdade de Engenharia da Universidade do Porto, Rua Dr. Roberto Frias, 4200-465 Porto, Portugal

Received 2 October 2006; received in revised form 18 December 2006; accepted 20 December 2006
Available online 30 December 2006

Abstract

Dead algal biomass is a natural material that serves as a basis for developing a new family of sorbent materials potentially suitable for many industrial applications. In this work an algal industrial waste from agar extraction process, algae *Gelidium* and a composite material obtained by immobilization of the algal waste with polyacrylonitrile (PAN) were physical characterized and used as biosorbents for dyes removal using methylene blue as model. The apparent and real densities and the porosity of biosorbents particles were determined by mercury porosimetry and helium picnometry. The methylene blue adsorption in the liquid phase was the method chosen to calculate the specific surface area of biosorbent particles as it seems to reproduce better the surface area accessible to metal ions in the biosorption process than the N_2 adsorption–desorption dry method. The porous texture of the biosorbents particles was also studied. Equilibrium isotherms are well described by the Langmuir equation, giving maximum uptake capacities of 171, 104 and 74 mg g^{-1}, respectively for algae, algal waste and composite material.

Kinetic experiments at different initial methylene blue concentrations were performed to evaluate the equilibrium time and the importance of the driving force to overcome mass transfer resistances. The pseudo-first-order and pseudo-second-order kinetic models adequately describe the kinetic data. The biosorbents used in this work proved to be promising materials for removing methylene blue from aqueous solutions.

Keywords: Methylene blue; Algal biomass; *Gelidium*; Biosorbent; Physical properties

1. Introduction

Effluents from textile, paper, plastics, leather, food, and other industries contain dyes or pigments used to colour their final products. The presence of these pollutants in water reduces light penetration and photosynthesis. In addition, some dyes are either toxic or mutagenic and carcinogenic [1]. The most commonly used methods for colour removal are coagulation and flocculation [2], biological oxidation and chemical precipitation [3] and activated carbon adsorption [4,5]. These technologies are effective and economical only for high dye concentrations. So, there is a growing interest in using low cost, commercially available materials for dyes adsorption. Adsorption of methylene blue (MB) has been studied using as adsorbents peanut hull [2], rice husk [3], ZMS-5-type zeolites and related silica polymorphs [6], clay from Turkey [7], magnesium silicate [8], water hyacinth roots [9], hexane-extracted spent bleaching earth [10], raw and activated date pits [11], guava seeds [12], perlite [13], algae *Sargassum muticum* [14], etc.

Marine algae *Gelidium* is used as raw material in the agar extraction industry. The process generates a large quantity of algal waste that can be used as low cost adsorbent. This algal waste, the algae *Gelidium* and an algal waste-based composite material were used efficiently to remove metal ions from aqueous solutions [15,16]. In this work, the same biosorbents were evaluated for MB removal.

Adsorbent physical characteristics, as surface area, porosity, size distribution and density have high influence in the adsorption process.

The MB adsorption method is currently used to measure the specific surface area of biosorbent particles in aqueous suspension. This method has been widely adopted for solids of variable nature such as iron oxides [17], clays [7], activated carbon [4,5], zeolites and silica [6]. The method has also been used to assess average pore size and pore size distribution in charcoals, silica, and alumina [18]. The Brunauer, Emmett, and Teller (BET) gas

* Corresponding author. Tel.: +351 22 508 1683; fax: +351 22 508 1674.
E-mail address: bventura@fe.up.pt (R.A.R. Boaventura).

0304-3894/$ – see front matter © 2006 Elsevier B.V. All rights reserved.
doi:10.1016/j.jhazmat.2006.12.055

adsorption method for dry surface area measurement [19] was also used in this work for comparison with MB results.

Meso and macroporosity, as well as the apparent density of biosorbents were measured by mercury porosimetry. Real densities were determined by helium picnometry.

The average grain size distribution of particles was obtained by scanning electron microscopy.

2. Materials and methods

2.1. Biosorbents

The adsorbents used in this study were an algal waste from the agar extraction industry, the same waste granulated by polyacrylonitrile (PAN) and algae *Gelidium*, the raw material for agar extraction.

Gelidium sesquipedale is a red algae harvested in the coasts of Algarve and São Martinho do Porto, Portugal. The industrial algal waste is composed essentially by 35% of algae *Gelidium* without agar and 65% of diatomaceous earth (≈72% SiO_2, 14% Al_2O_3, 8.8% K_2O, 4% Na_2O and 1.2% of other elements) used as filtration aid in the extraction process. The algal waste and algae *Gelidium* were previously air-dried to remove odours and most water. After 2 days, were dried at 60 °C and then crushed (mill Retsch, model ZM 100). Algae *Gelidium* particles were sieved (AS200 digit Retsch shaker) to separate the 0.25–1 mm fraction.

To prepare the granulated material (composite particles), fibrous PAN was dissolved in DMSO (dimethyl sulfoxide) during 1–2 h. The powdered active component (industrial algal waste) was gradually added to PAN solution under stirring and the suspension mixed for about 30 min. Homogeneous suspension was then dispersed into water (coagulation bath) at room temperature. Beads formed in water were washed with distilled water, separated by filtration on Buchner funnel and dried at about 30–40 °C. Dry product was then sieved. According to the procedure used, dry beads contain 75% of the active component (algal waste).

2.2. Physical characterization

2.2.1. Scanning electron microscopy (SEM)

SEM (JEOL JXA-840 operated a 30 keV acceleration potential) was selected to elucidate the particle size and porous properties of the biosorbents particles. Prior to the observation, the surface of the samples was coated with a thin, electric conductive gold film.

2.2.2. Grain size distribution

The grain size distribution of the spherical and thin plate particles were carried out in a Coulter Counter (LS Particle Size Analyzer) and by microscopy image observation, respectively.

2.2.3. Real and apparent densities, porosity, pore volume and pore size distribution

Real densities of biosorbents were calculated by helium picnometry (ACCUPYC 1330). Apparent densities, porosity, pore volume and pore size distribution, were obtained from mercury porosimetry measurements (Micromerities Poresizer 9320).

2.2.4. Surface area

The surface are of the biosorbents was determined by the methylene blue adsorption method, mercury intrusion method and BET method (ASAP 2000 apparatus), based on nitrogen adsorption–desorption isotherms at 77 K, respectively.

2.3. Preparation of MB solution

MB stock solution was prepared by dissolving a weighed quantity of $C_{16}H_{18}ClN_3S{\cdot}2H_2O$ (Merck, Darmstadt) in distilled water. MB solutions in range of 40–800 mg l^{-1} were obtained by diluting the stock solution.

2.4. Sorption kinetic studies

In order to determine the contact time required to reach adsorption equilibrium, batch experiments were performed for different initial MB concentrations at pH 6.0. Temperature was controlled by a thermostatic bath and monitored throughout each experiment (temperature meter WTW 538) ($T = 20$ °C). A vessel was filled with 1 l of MB solution, then a known weight of biomass was added and the suspension stirred (magnetic stirrer Heidolph MR 3000) at 600 rpm. Samples of 5 ml were taken at pre-defined time intervals ranging from 1 to 10 min after the addition of MB solution. More frequent samples were taken at the beginning of each experiment. Samples were centrifuged (Eppendorf Centrifuge 5410) and the supernatant was removed for analysis of MB.

2.5. Sorption equilibrium studies

The experiments were conducted in duplicate, using 100 ml Erlenmeyer flasks, at $T = 20$ °C and pH 6.0. The initial concentration varied between 40 and 800 mg MB l^{-1}. A known weight of material was suspended in 100 ml of MB solution and stirred at 100 rpm. Temperature was maintained constant by using a HOTECOLD-M (Selecta) thermostatic refrigerator. Once equilibrium was reached, 3 h later, samples were taken and centrifuged (Eppendorf Centrifuge 5410) and the supernatant analysed for the remaining MB.

2.6. Analytical procedure

MB concentration was determined by measuring the absorbance at 650 nm (UV–vis, PYE UNICAM-PU 8600 spectrophotometer). This wavelength corresponds to the maximum absorption peak of the MB monomer [20].

The amount of MB adsorbed per gram of biosorbent was calculated as:

$$q = \frac{V(C_i - C_f)}{W} \quad (1)$$

where q is the MB uptake (mg MB g^{-1} of the biosorbent), C_i and C_f the initial and final MB concentrations in solution (mg l^{-1}), V

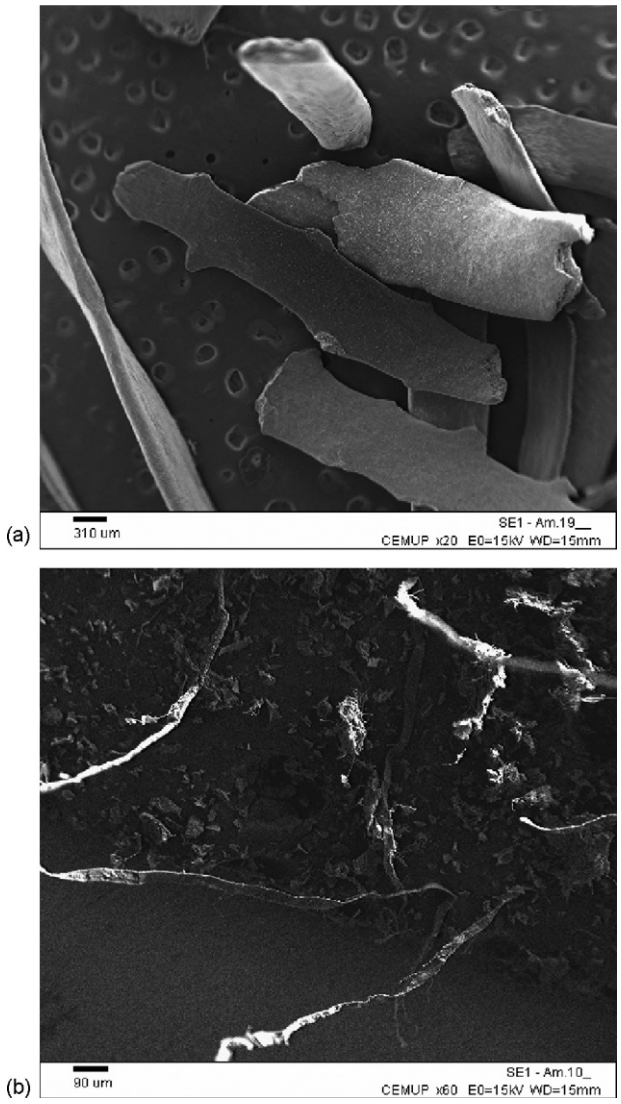

Fig. 1. Scanning electron microscopy of algae *Gelidium* (a) and algal waste after agar extraction (b).

the volume of solution (l), and W is the dry weight of the added biosorbent (g).

2.7. Parameters estimation

The experimental data obtained from equilibrium and kinetic studies were fitted to mathematical models by a non-linear regression method (FigSys for Windows from BIOSOFT). Model parameters were obtained by minimizing the sum of the squared deviations between experimental and predicted values. Model goodness was evaluated by the standard deviations, sum of square residuals (S_R^2) and regression coefficients (R^2). Model performances were compared by the F-test.

3. Results and discussion

3.1. Particle size

Fig. 1(a and b) present micrographs of algae *Gelidium* before and after agar extraction obtained by scanning electron microscopy (SEM). Particles are like thin plates, with a length and width that greatly exceed the thickness. Algae *Gelidium* filaments after agar extraction can be distinguished in the waste (Fig. 1(b)). The histograms presented in Fig. 2(a and b) were obtained from algae *Gelidium* image analysis (fraction size 0.5–0.85 mm). An equivalent length and width of, respectively, 2.5 ± 0.7 and 0.6 ± 0.1 mm were calculated from the histograms. Thickness was determined by SEM (Fig. 2(c)). The equivalent thickness was around 0.1 mm.

Fig. 3(a) presents the grain size distribution of fractions 0.5–1.0 and 1.0–2.0 mm of the granulated waste given by a Coulter Counter (LS Particle Size Analyzer). An average equivalent spherical diameter of 903 μm obtained for the first fraction is comparable to values from scanning electron microscopy (884 and 923 μm) (Fig. 3(b and c)). The median equivalent spherical diameter for the higher grain size fraction was 1425 μm.

3.2. Physical characterization

Real densities of biosorbents were calculated by helium picnometry (ACCUPYC 1330), and results are presented in Table 1.

Mercury porosimetry measurements (intrusion and extrusion) were performed using a Micromerities Poresizer 9320, at a pressure range between 0.5 and 30.000 psia, which allows the measurement of total pore volume of pores with diameters between 360 μm and 60 Å. Mercury only penetrates sample pores for pressures higher than 0.15 psia. The volume of mercury (V_{Hg}) necessary to fill the penetrometer is given by:

$$V_{Hg} = \frac{m_{penet+sample+Hg} - (m_{penet} + m_{sample})}{\rho_{Hg}} \quad (2)$$

where m_{penet} is the weight of the penetrometer empty, m_{sample} the mass of material added to the penetrometer, $m_{penet+sample+Hg}$ the total mass of penetrometer filled with sample and mercury and ρ_{Hg} is the mercury density.

The apparent density was calculated as:

$$\rho_{ap} = \frac{m_{sample}}{V_{sample}} = \frac{m_{sample}}{V_{penet} - V_{Hg}} \quad (3)$$

and the obtained values are presented in Table 1. Fig. 4(a–c) presents the mercury cumulative intrusion and extrusion volume as a function of the pore diameter, respectively for the composite material, algal waste and algae *Gelidium*. The results for intruded mercury (V_{Hg}) are presented in Table 1. High values are associated with high grain sizes of the composite material. The lower intruded volume corresponds to algae *Gelidium*.

Specific surface areas (Table 1) were calculated by integrating the curve of penetrated volume as a pressure function and assuming a constant transversal area for the pores [21].

Particle porosity (ε_p) is defined as the void space:

$$\varepsilon_p = \frac{V_P}{V_P + V_S} \Rightarrow 1 - \varepsilon_p = \frac{V_S}{V_P + V_S} \quad (4)$$

Taking into account that

$$\rho_{ap} = \frac{m_S}{V_P + V_S} \Rightarrow V_P + V_S = \frac{m_S}{\rho_{ap}} \quad (5)$$

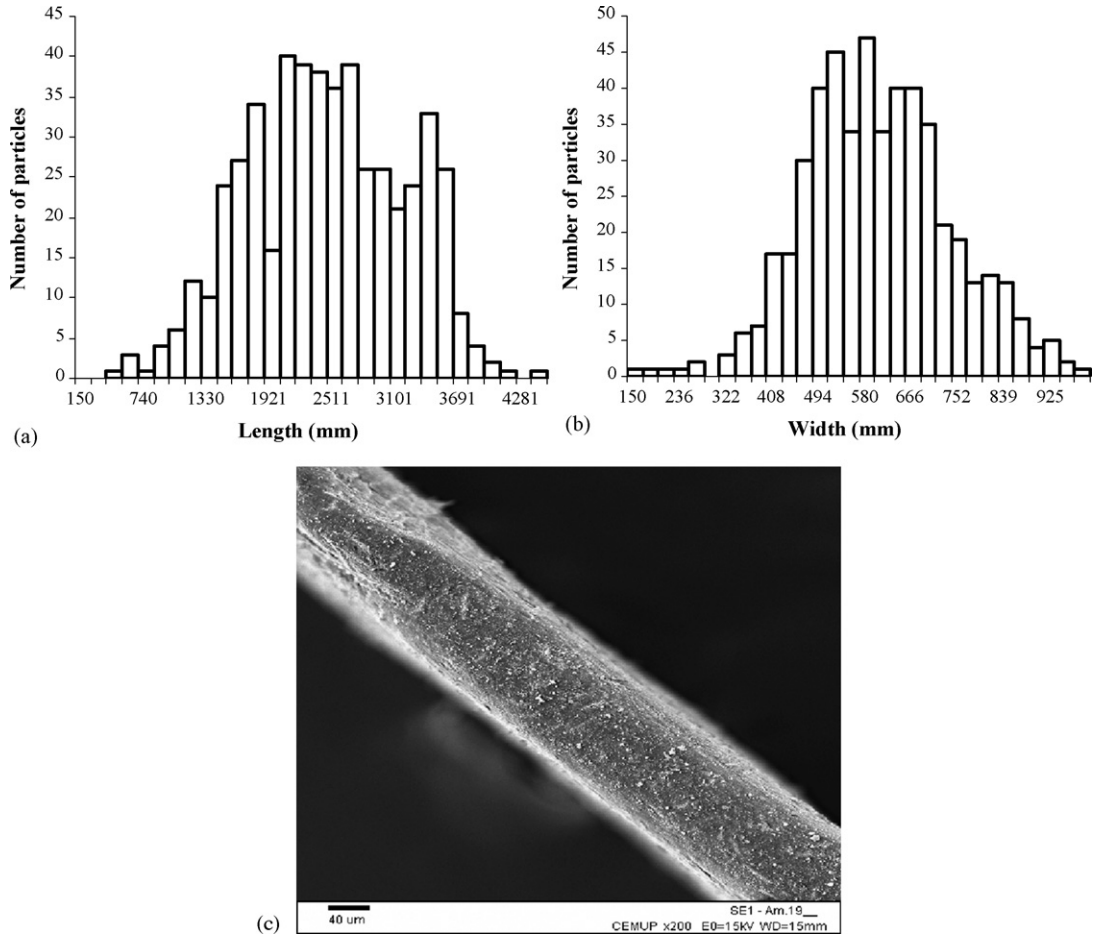

Fig. 2. Grain size distribution of algae *Gelidium* particles (a), length (b) and width and thickness (c).

and

$$\rho_{re} = \frac{m_S}{V_S} \Rightarrow V_S = \frac{m_S}{\rho_{re}} \quad (6)$$

where V_P is the pore volume, V_S the solid volume, ρ_{re} the real density and m_S is the mass of real solid.

Porosity is related to real and apparent densities by the expression:

$$\varepsilon_p = 1 - \frac{\rho_{ap}}{\rho_{re}} \quad (7)$$

Algae *Gelidium* has low porosity, because real and apparent densities are similar. This suggests that the sample cannot tolerate a high pressure without collapsing or compressing. The apparent density of the other materials is lower than the real one, suggesting the presence of pores smaller than 60 Å.

Pore size distributions are presented in Fig. 5(a–c), respectively for composite material, algal waste and algae *Gelidium*. The composite material presents a bimodal distribution with similar average diameters (10 and 4 μm), and an equitable distribution for particles with diameters in the range 0.5–1.0 mm. Small volumes of macropores (average diameter 200 nm) and mesopores (10 nm) have also been observed on the distribution curves. The intrusion curve presents an increase in two size ranges, namely between 100 and 7 μm and between 6 and 1 μm. The intrusion of mercury between 1 and 0.1 mm pore size is due to the interparticle space. Thus, the results will be affected by an excess of mercury volume.

For the algal waste, the type of curve indicates a porous sample not consolidated, constituted by untied particles, being a

Table 1
Physical properties

Biosorbent	V_{Hg} (cm^3 g^{-1})	ρ_{ap} (g cm^{-3})	ρ_{re} (g cm^{-3})	ε_p	d_e (μm)	d_V (μm)
Algae *Gelidium*	0.1256	1.342	1.46	0.08	0.04	1.4
Algal waste	1.416	0.413	1.97	0.79	0.36	5.6
Composite material ($1.0 < d_p < 2.0$) mm	3.468	0.219	1.64	0.85	0.35	4.3
Composite material ($0.5 < d_p < 1.0$) mm	2.735	0.249	1.64	0.87	0.23	8.4

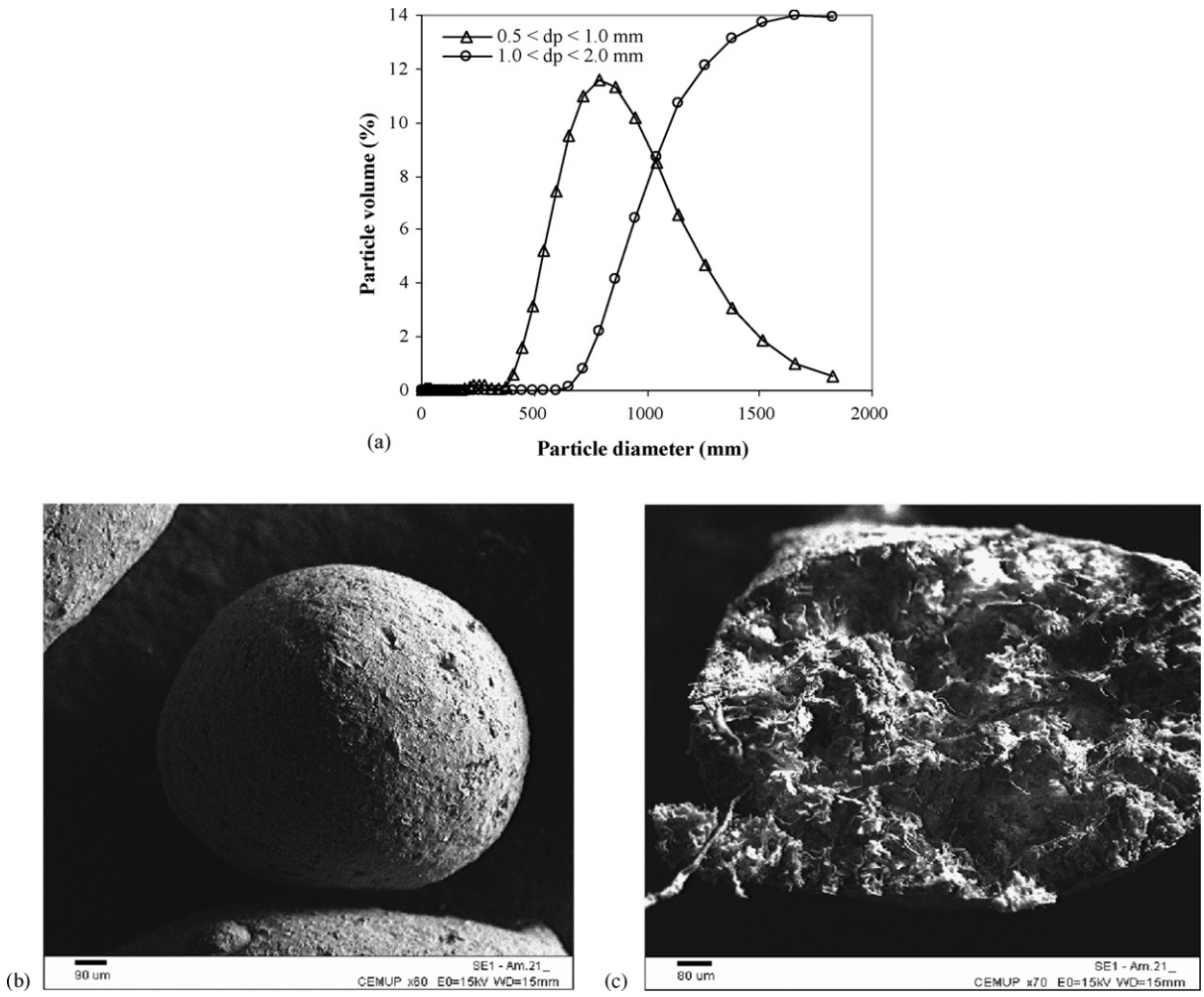

Fig. 3. (a) Grain size distribution of the composite material obtained by the Coulter Counter. Frontal (b) and cross-sectional (c) scanning electron micrographs of beads containing algal waste biomass immobilized in polyacrilonitrile.

part of the porous space between particles [22]. The intrusion curve presents a linear increase in the range 300–15 μm, and an accentuated increase between 15 and 2 μm. Algal waste has a bimodal distribution of macropores (9 and 4 μm) or a wide unimodal distribution.

For the algae *Gelidium* we can observe a high increase of the mercury intrusion between 200 and 8 μm, due the occupation of interparticle spaces. Between 8 and 0.1 μm the intrusion curve presents a linear increase with pressure, which is often interpreted as the collapse of the porous structure [22]. Therefore, it presents a non-rigid structure. Fig. 5(c) suggests a bimodal distribution of macropores (10 and 1 μm) or a wide unimodal distribution. For pores diameter lower than 0.1 μm, the porous structure collapsed.

Considering cylindrical pores as in the mercury porosimetry method, the equivalent diameter, d_e, presented in Table 1 suggests a macroporous material.

The apparent density can be defined as:

$$\rho_{ap} = \frac{m_S}{V_S + V_{P\geq 60} + V_{P<60}} \tag{8}$$

where the total volume of pores is the sum of the pores higher than 60 Å ($V_{P\geq 60}$) and lower than 60 Å ($V_{P<60}$).

The specific intrusion volume represents the quantity of mercury that penetrates in pores with a diameter higher than 60 Å, and is defined as:

$$V_{Hg} = \frac{V_{P\geq 60}}{m_S} \tag{9}$$

If we do not consider the pores lower than 60 Å, the apparent density of the composite material ($0.5 < d_p < 1.0$ mm) can be calculated as:

$$\rho^*_{ap} = \frac{m_S}{V_S + V_{P\geq 60\,Å}} = \frac{1}{1/\rho_{re} + V_{Hg}} = 0.299\ \text{g/cm}^3 \tag{10}$$

Using Eq. (8), and the values presented in Table 1, the specific volume of pores with diameter lower than 60 Å is obtained as:

$$0.249\ \text{g/cm}^3 = \frac{1}{1/1.64 + 2.735 + V'_{P<60\,Å}} \Rightarrow V'_{P<60\,Å} = 0.671\ \text{cm}^3/\text{g} \tag{11}$$

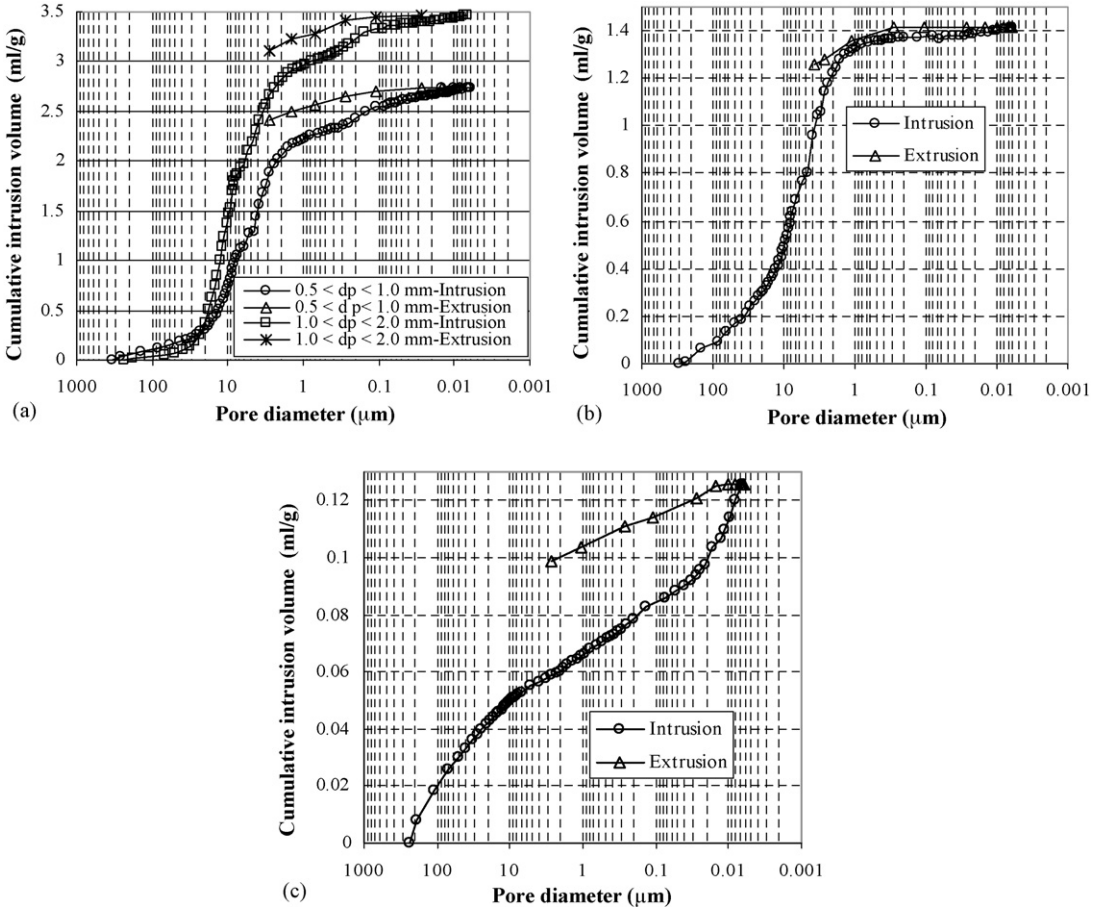

Fig. 4. Cumulative volume of mercury intruded/extruded: (a) composite material, (b) algal waste and (c) algae *Gelidium*.

The apparent density of the composite material, excluding the specific volume of pores higher than 60 Å, is given by:

$$\rho_{ap}^{**} = \frac{m_S}{V_S + V_{P<60\,Å}} = \frac{1}{1/\rho_{re} + V'_{P<60\,Å}} = 0.78\,g/cm^3 \quad (12)$$

Values shown in Table 2 allow to say that the algal waste and the composite material have respectively, 26.0, 12.3 (higher size fraction) and 19.7% (lower size fraction) of pores with a diameter lower than 60 Å. For algae *Gelidium* it is impossible to determine the pores volume for a diameter lower than 60 Å. This is due to the non-rigid structure of the particles, which collapse with mercury penetration. The apparent density is similar to the real density, which indicates a low porosity. However, scanning electron microscopy (Fig. 6) shows a high surface porosity of the algae *Gelidium* particles, with 2.0 μm average diameter macropores, which is similar to the median pore diameter (volume), d_V, obtained by mercury porosimetry. The equivalent pore diameter, d_e, considering cylindrical pores are lower because is calculated from the mercury intruded and the specific surface area, which may be underestimated. The algal waste and the composite material present values of d_V higher than algae *Gelidium*, due to treatment of the algae for agar extraction and also, in the case of the composite material, due to immobilization with PAN, which results in a higher porous structure.

3.3. Methylene blue (MB) adsorption

3.3.1. Equilibrium

Classical Langmuir and Langmuir–Freundlich sorption models have been used to describe equilibrium between adsorbed MB concentration (q_{eq}) and solution concentration (C_{eq}), at constant temperature [5,23]. The Langmuir model assumes that all adsorbed species interact only with a site, so, adsorption is limited to a monolayer and adsorption energy is identical for all sites and independent of the presence of adsorbed species on neighbouring sites. The model is represented by the following equation [24]:

$$q_{eq} = \frac{q_{max} K_L C_{eq}}{1 + K_L C_{eq}} \quad (13)$$

where q_{max} is the maximum amount of MB per unit weight of biosorbent to form a complete adsorbed MB monolayer and K_L is a coefficient related to the affinity between the sorbent active sites and adsorbate. The Langmuir–Freundlich (LF) isotherm, derived from the Langmuir and Freundlich models, is an empirical model represented by the following equation [25]:

$$q_{eq} = \frac{q_{LF} K_{LF} (C_{eq})^{1/n}}{1 + K_{LF} (C_{eq})^{1/n}} \quad (14)$$

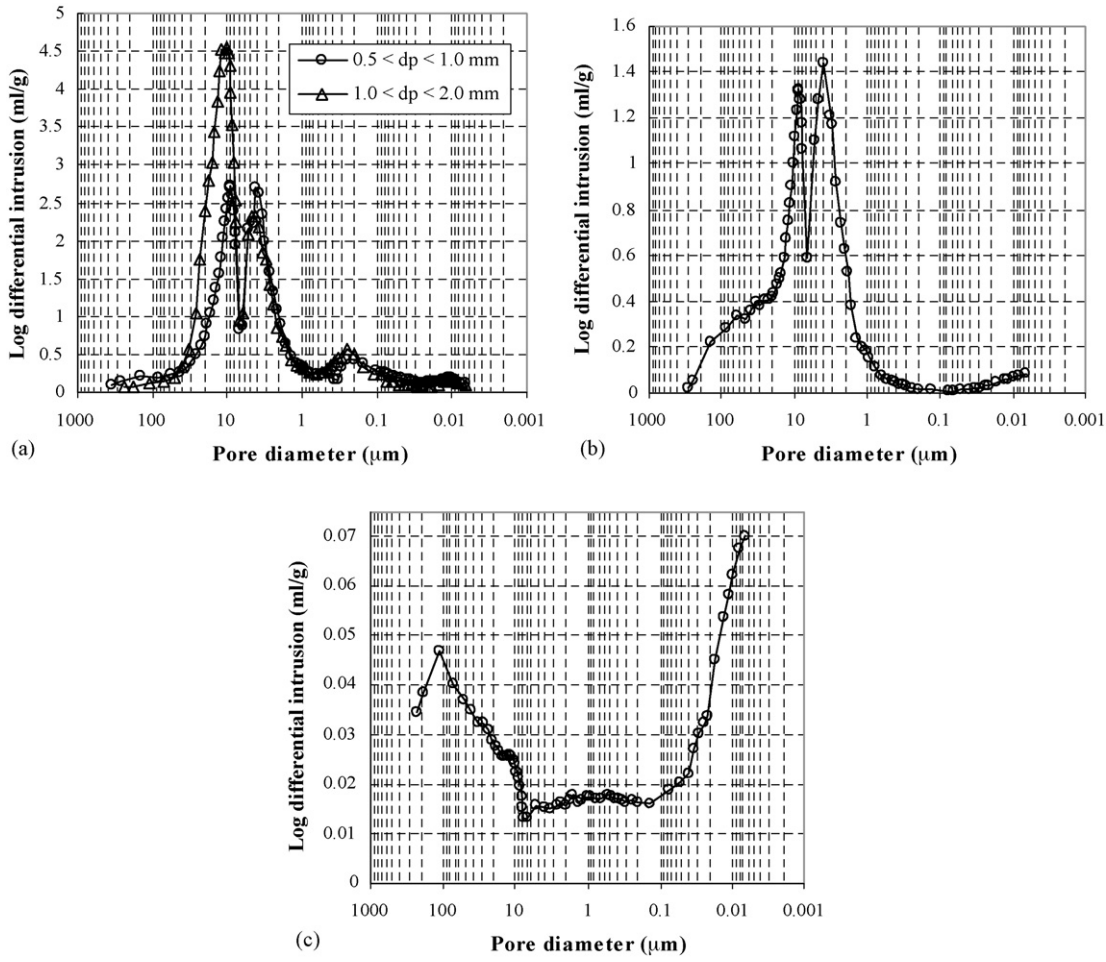

Fig. 5. Pore size distribution of adsorbent materials: (a) composite material, (b) algal waste and (c) algae *Gelidium*.

where K_{LF} ($l^{1/n}\,mg^{-1/n}$), q_{LF} ($mg\,g^{-1}$) and n (dimensionless) are the three adjustable empirical parameters. If $n = 1$ Eq. (14) becomes the Langmuir equation.

Experimental data are well correlated with the predicted by the Langmuir and Langmuir–Freundlich models (Fig. 7). The adequacy of the two models was compared by using the statistical F-test (Table 3). Results for a 95% confidence level show that the difference is not significant. So, the results will be discussed on the basis of Langmuir parameters.

Obtained values for q_{max} ($mg\,MB\,g^{-1}$ biosorbent) and K_L ($l\,solution\,mg^{-1}$ MB) (Table 3), suggest that algae *Gelidium* be a better biosorbent for MB than algal waste and composite material.

Table 4 compares MB sorption on different sorbents, and shows that biosorbents used in this work present good performance in MB removal.

Studied biosorbents are characterized by an heterogeneous distribution of negatively charged carboxylic and hydroxyl groups [26]. In aqueous solution MB molecule is cationic, so, adsorption can be due to the electrostatic interaction between the negative charged groups present in the materials and the positive charge of the MB molecule. The adsorption of MB by macroalga was studied for pH values in the range 1–10 [14]. The authors concluded that the uptake capacity was unaffected in the pH range 4–10 but impaired at low pH. The same results were obtained by other investigators [13,23] At low pH values

Table 2
Apparent density ρ_{ap}^{*} and ρ_{ap}^{**} and volume of pores lower than 60 Å

Biosorbent	V_P'(total) ($cm^3\,g^{-1}$)	ρ_{ap}^{*} ($g\,cm^{-3}$)	$V'_{P<60\,Å}$ ($cm^3\,g^{-1}$)	ρ_{ap}^{**} ($g\,cm^{-3}$)
Algae *Gelidium*	0.126	1.234	–	1.614
Algal waste	1.914	0.520	0.498	0.994
Composite material ($1.0 < d_p < 2.0$) mm	3.956	0.245	0.488	0.92
Composite material ($0.5 < d_p < 1.0$) mm	3.406	0.299	0.671	0.78

Table 3
Estimated parameters for Langmuir and Langmuir–Freundlich models (value ± standard deviation)

Biosorbent	Langmuir parameters		DF[a]	R^2	S_R^2 (mg g^{-1})^2	F_{cal}	$F_{1-\alpha}$
	q_{max} (mg g^{-1})	K_L (l mg^{-1}) × 10^2					
Gelidium	171 ± 3	7.9 ± 0.8	18	0.982	73.8	2.1	3.3
Algal waste	104 ± 2	6.7 ± 0.7	18	0.965	36.0	1.0	3.3
Composite material	74 ± 2	8.1 ± 0.8	18	0.962	15.9	1.1	3.3

Biosorbent	Langmuir–Freundlich parameters		DF[a]	R^2	S_R^2 (mg g^{-1})^2
	q_{LF} (mg g^{-1})	K_{LF} (l$^{1/n}$ mg$^{-1/n}$) × 10^2			
Gelidium	162 ± 3	4.2 ± 0.8	17	0.991	35.3
Algal waste	107 ± 5	9 ± 2	17	0.967	36.3
Composite material	78 ± 4	13 ± 3	17	0.966	14.9

[a] Degrees of freedom.

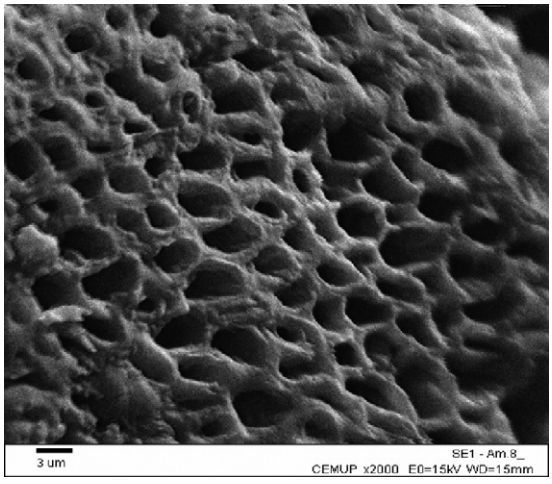

Fig. 6. Scanning electron microscopy of pores of the thin plate particles (*Gelidium*).

binding sites are protonated and an important amount of MB is adsorbed, suggesting that electrostatic and hydrophobic interactions are both important contributions for MB adsorption [14,27].

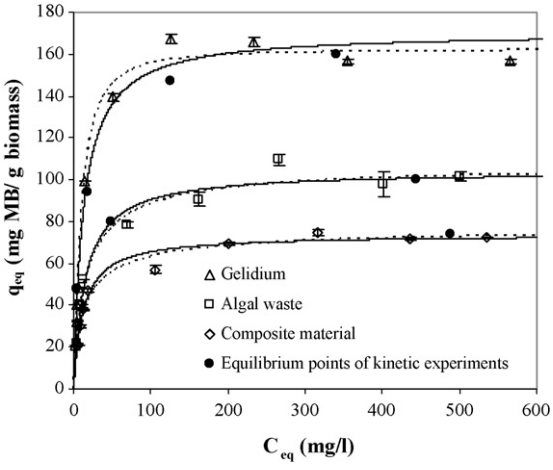

Fig. 7. MB biosorption isotherms for algae *Gelidium*, algal waste and composite material. Solid lines—Langmuir model; dotted lines—Langmuir–Freundlich model.

3.3.2. Specific surface area

It has been assumed that MB forms a monolayer of adsorbed molecules onto the surface of sorbent particles, which permits to calculate the specific surface area as:

$$S_{MB} = \frac{q_{max} a_{MB} N}{M_{MB}} \quad (15)$$

where S_{MB} is the specific surface area (m^2 g^{-1}), q_{max} the mass of adsorbed MB in the monolayer (g$_{MB}$ g^{-1}), a_{MB} the area occupied by one MB molecule (m^2 molecule^{-1}), N the Avogadro's number (6.02×10^{23} molecule mol^{-1}) and M is the MB molar mass (355.89 g mol^{-1}).

The MB molecule has a parallelepiped shape with approximately 17 Å × 7.6 Å × 3.25 Å. The biosorbent area covered by one MB molecule may change because attachment may be done with different orientations: (i) if the molecule lies on its largest face on the sorbent surface, the covered area is about 130 Å^2 per molecule [28–30]; (ii) if the molecule is tilted (65–70°) with the respect to the surface, the covered area is about 66 Å^2 per molecule [31]; and (iii) if the longest axis is oriented perpendicular to the surface, the covered area is about 24.7 Å^2 per molecule [32]. The uncertainty in the assumption of the covered area can affect the estimation of specific surface by more than 100%. The most common assumption is that the molecule lies flat on the

Table 4
Maximum uptake capacity of MB on several adsorbents

Adsorbent	q_{max} (mg g^{-1})	Reference
Activated carbon	373.9	[5]
Algae *Sargassum muticum*	279.2	[14]
Cottom waste	240	[42]
Hydrilla verticillata	198	[43]
Moss	185	[9]
Algae *Gelidium*	171	Present work
Perlite	162.3	[13]
Spirodela polyrrhiza (duckweed)	144.9	[23]
Water hyacinth root	128.9	[9]
Algal waste	104	Present work
Carbonised spent bleaching earth	94.5	[10]
Date pits	80.3	[11]
Composite material	74	Present work
Zeolite	53.1	[13]

Table 5
Specific surface area calculated by methylene blue and BET methods (value ± standard deviation)

Biosorbent	Methylene blue method (MB)		BET method (N_2)	Mercury intrusion
	A_{sp} ($m^2\,g^{-1}$)		A_{sp} ($m^2\,g^{-1}$)	A_{sp} ($m^2\,g^{-1}$)
	a_{MB} ($Å^2$) = 24.7	a_{MB} ($Å^2$) = 130		
Algae *Gelidium*	71 ± 2	375 ± 8	0.23 ± 0.01	13.5
Algal waste	44 ± 1	229 ± 5	1.37 ± 0.02	15.8
Composite material ($0.5 < d_p < 1.0$ mm)	31 ± 1	162 ± 3	13.1 ± 0.2	39.7
Composite material ($1.0 < d_p < 2.0$ mm)	–	–	9.7 ± 0.1	47.1

biomass surface on its largest face; in this case, the area covered by one MB molecule is about 130 $Å^2$. Table 5 presents the values of the specific surface area, assuming that one MB molecule covers 24.7 and 130 $Å^2$ of the biosorbent surface.

The nitrogen adsorption technique was also used to study biosorbents surface. Fig. 8(a and b) shows N_2 adsorption–desorption isotherms for the biosorbents. These isotherms cannot be rigorously classified into any IUPAC group [33]. The initial part corresponds to type II, typical of non-porous or macroporous materials, and represents a process of monolayer–multilayer adsorption. On the other hand, it can be seen (Fig. 8(a and b)) a hysteresis loop in multilayer range,

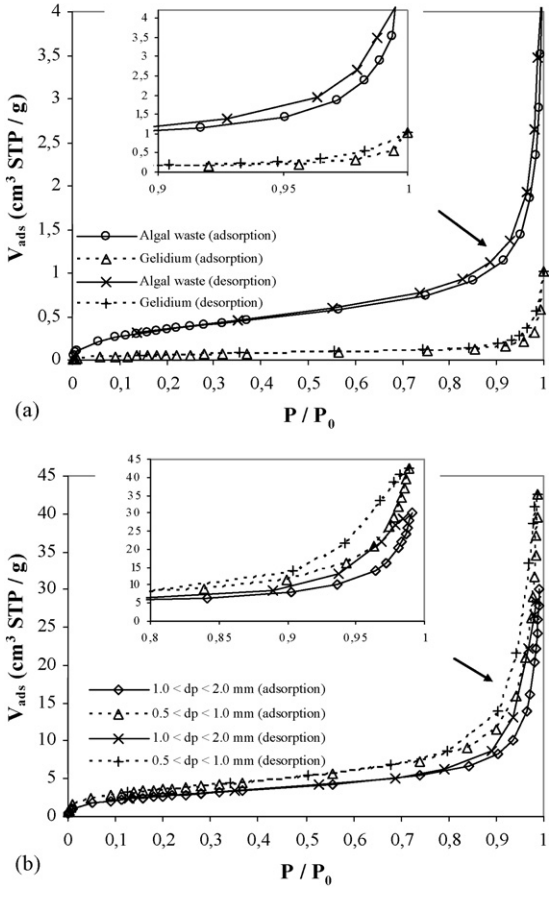

Fig. 8. Nitrogen adsorption–desorption isotherms: (a) algae *Gelidium* and algal waste and (b) composite material.

associated with capillary condensation in mesopores, which is characteristic of type IV isotherms [34]. So, isotherms can be classified into group IIb if the new classification system proposed by [35] is used. The hysterese loop can be classified into type H-3 [36]. This is typical of aggregated particles that form plates and give rise to formation of such rifts or wedges. The closure of the loop is gradual, and this confirms the existence of mesopores formed by parallel plates or wedge-shaped sites where desorption occurs due to capillary evaporation. The point of closure (0.8, 0.7, 0.8 and 0.9, respectively for composite material (smaller and larger particles), algal waste and composite material), is attributed to the surface tension of the liquid adsorbate reaching an unstable state at a specific pressure [37].

The BET equation (Eq. (16)) represents the general shape of actual experimental isotherms. From these isotherms the volume of gas required to form a unimolecular layer of gas on adsorbent surface can be computed:

$$\frac{P}{V_{ads}(P_0 - P)} = \frac{1}{V_m c} + \frac{c-1}{V_m c}\frac{P}{P_0} \tag{16}$$

where P is the applied pressure (mmHg), P_0 the saturation pressure (it is near atmospheric pressure for nitrogen at 77 K) (760 mmHg), V_{ads} the volume of gas adsorbed at P/P_0 (cm^3 STP mol^{-1}), V_m the volume of adsorbate for one monolayer of surface coverage (cm^3 STP mol^{-1}), and c is related to the heat of adsorption in the first and subsequent adsorbed layers. Plots of $P/[V_{ads}(P_0 - P)]$ versus P/P_0 yield straight lines for P/P_0 in the range 0.05–0.3 (Fig. 9(a and b)). The slope and intercept can be used to determine V_m and c. The adsorbent surface area, A_{BET} ($m^2\,g^{-1}$) is calculated by the expression:

$$A_{BET} = \frac{V_m a_m N}{V_M^g} \tag{17}$$

where a_m is the area occupied by a nitrogen molecule ($0.162 \times 10^{-18}\,m^2$ molecule^{-1}), N the Avogadro constant (molecules mol^{-1}) and V_M^g is the molar standard volume of the gas at the standard pressure (P_S = 101325 Pa) and standard temperature (T_S = 273.15 K). V_M^g is given by $V_M^g = RT_s/P_s = 22.7 \times 10^3\,cm^3$ STP mol^{-1} (R is the general gas constant for ideal gases, 8.314 Pa m^3 mol^{-1} K^{-1}).

Table 5 presents surface area values obtained by the three techniques. The methylene blue technique involves high bonding energy (ionic Coulombian attraction–chemisortpion) and is generally limited to a monolayer. In the gas absorption method,

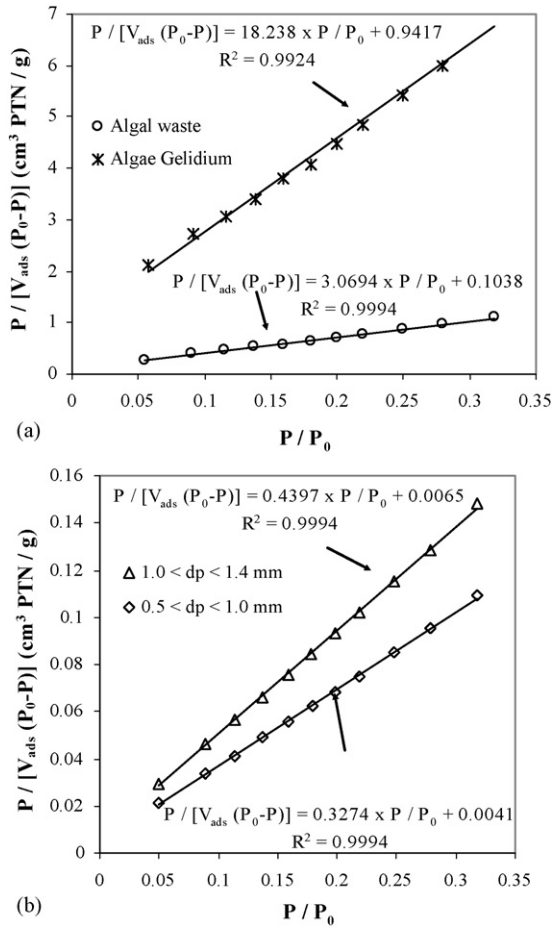

Fig. 9. Linear relationship between $P/[V_{ads}(P_0 - P)]$ and P/P_0 (Eq. (15)): (a) algae *Gelidium* and algal waste and (b) composite material.

gas molecules are attracted to the surface by van der Waals forces (physisorption), and multiple layers may form, such as in the BET theory.

Specific surface area obtained by mercury porosimetry for the composite material is of the same magnitude as the obtained by the methylene blue method. For algal waste and algae *Gelidium*, mercury porosimetry gives lower values. This is related to the collapse of the porous non-rigid structure. Mercury porosimetry gives higher pore volumes than N_2 adsorption suggesting that the BET method cannot be applied to this kind of materials.

Results obtained by the MB method better reflect biosorbents surface area available for metal adsorption. As the uncertainty in the assumption of the covered area can strongly affect the estimation of specific surface, the results can only be used to compare the three biosorbents. The same limitation has been pointed out by other authors. Santamarina et al. [38] obtained higher specific surface area for swelling clays using MB adsorption method, because interlayer surfaces could be reached by exchangeable ions after hydration (montmorillonite, Fuller's earth, and Mexico City clay). However, for nonswelling clay minerals, such as kaolinite, the same authors didn't find any difference in specific surface area determined by dry or wet methods.

HE and Tebo [39] obtained higher surface area for SG-1 spores by the MB method, suggesting that in the water-wet state, a spore is swollen and there is a water-filled porous structure. When the pore is air-dried or even freeze-dried, this porous structure collapses, resulting in a much smaller surface area. Even molecules as small as nitrogen are unable to get in. The specific area of wet SG-1 spores was 74.7 $m^2\,g^{-1}$ of dry weight as measured by the methylene blue adsorption method, using $a_{MB} = 55$ (Å)^2, whereas by the N_2 adsorption method it was only 7 $m^2\,g^{-1}$ of dry weight.

The same trend was observed by Kaewprasit et al. [40] in the determination of the specific surface area of cotton fiber, where all the pores are closed in the vacuum-dried state, which promotes the formation of interchain hydrogen linkages or cellulose–cellulose linkages which are too strong to be replaced by N_2 molecules. The specific surface area of *Sargassum muticum* was determined by Rubin et al. [14] using methylene blue and BET methods. Assuming the area of the methylene blue molecule as 108 (Å)^2, the surface area was about 400 $m^2\,g^{-1}$. This value is much higher than that found using the BET method (2.86 $m^2\,g^{-1}$).

3.3.3. Kinetics experiments

Adsorption of MB occurs mainly within the first 60 min for algae *Gelidium* (Fig. 10(a)) and 20 min for algal waste and composite material (Fig. 10(b)). MB removal from solution increases as the initial concentration decreases. Similar results were obtained in the removal of MB by the macroalga *Sargassum muticum* [14]. The highest percentage removal at saturation was found to be 96% ($C_i = 101$ mg l^{-1}; $C_f = 5$ mg l^{-1}) for algae *Gelidium*. For the initial concentration of approximately

Table 6
Estimated parameters for the pseudo-first-order model at different initial MB concentrations (value ± standard deviation)

Biosorbent	C_i (mg l^{-1})	q_{eq}[a] (mg g^{-1})	Pseudo-first-order model				
			q_{eq} (mg g^{-1})	$k_{1,ads}$ (min^{-1}) × 10^2	R^2	S_R^2 (mg g^{-1})^2	$r_{ads}(i)$ (mg g^{-1} min^{-1})
Gelidium	658	159.5	156 ± 2	4.2 ± 0.3	0.991	31.9	6.6 ± 0.4
	420	147.1	142 ± 2	4.0 ± 0.2	0.993	20.9	5.7 ± 0.3
	206	93.8	94.0 ± 0.3	5.5 ± 0.1	0.999	0.7	5.2 ± 0.1
	101	47.5	47.8 ± 0.2	6.8 ± 0.1	0.999	0.2	3.3 ± 0.1
Algal waste	644	100.0	93 ± 3	110 ± 30	0.916	83.2	102 ± 28
	209	78.5	76 ± 2	70 ± 14	0.966	22.5	61 ± 11
Composite material	635	73.6	70 ± 2	23 ± 3	0.976	16.2	16 ± 2

[a] Experimental equilibrium uptake data.

Table 7
Estimated parameters for the pseudo-second-order model at different initial MB concentrations (value ± standard deviation) and *F*-test

Biosorbent	C_i (mg/l)	q_{eq}[a] (mg g^{-1})	Pseudo-second-order model					*F*-test		
			q_{eq} (mg g^{-1})	$k_{2,ads}$ (g mg^{-1} min^{-1}) × 10^4	R^2	S_R^2 (mg g^{-1})^2	$r_{ads}(i)$ (mg g^{-1} min^{-1})	F_{cal}	$F_{1-\alpha}$	Statistically better
Gelidium	658	159.5	182 ± 3	2.9 ± 0.2	0.995	15.1	9.7 ± 0.8	2.1	1.9	2nd order
	420	147.1	167 ± 1	2.9 ± 0.1	0.999	1.7	8.1 ± 0.3	12.7	1.9	2nd order
	206	93.8	107 ± 2	6.7 ± 0.1	0.992	10.0	7.7 ± 0.8	16.1	1.9	1st order
	101	47.5	53.3 ± 0.8	18 ± 1	0.990	2.7	5.0 ± 0.5	13.8	1.9	1st order
Algal waste	644	100.0	97.0 ± 0.3	148 ± 5	0.950	49.4	137 ± 45	1.7	2.3	No difference
	209	78.5	79 ± 1	135 ± 16	0.993	4.8	84 ± 10	4.7	2.3	2nd order
Composite material	635	73.6	75 ± 2	50 ± 7	0.989	6.9	27 ± 4	2.3	2.2	2nd order

[a] Experimental equilibrium uptake data.

600 mg l^{-1}, percentage removals were 48, 32 and 23%, respectively for algae *Gelidium*, algal waste and composite material. Removal of MB molecules is faster at the initial stage as the driving force is higher, which permits to overcome all external mass transfer resistances, and higher affinity active sites are first occupied. After that, MB concentration in solution decreases, and the remaining active sites, with lower affinities, are occupied slowly.

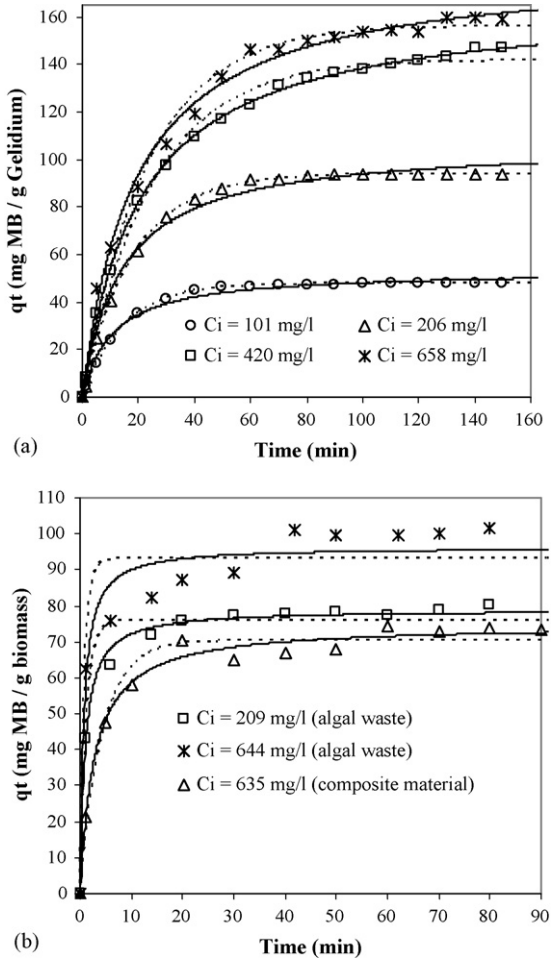

Fig. 10. Evolution of adsorbed MB concentration on algae *Gelidium* (a) and algal waste and composite material (b) with contact time for different values of the initial concentration (C_i). Solid lines—peudo-first-order model; dotted lines—pseudo-second-order model.

The sorption kinetic models used in this study are based on the Ritchie equation, assuming that a number of surface sites, *n*, are occupied by each MB cation. From the general form of the Ritchie equation, it is possible to deduce the pseudo-first-order and pseudo-second-order kinetic models [41]:

Pseudo-first-order model:

$$q_t = q_{eq}[1 - \exp(-k_{1,ads}t)] \quad (18)$$

Pseudo-second-order model:

$$q_t = \frac{q_{eq}^2 k_{2,ads} t}{1 + k_{2,ads} q_{eq} t} \quad (19)$$

where q_t is the concentration of ion species in the sorbent at time t (mg MB g^{-1} biosorbent), $k_{1,ads}$ is the biosorption constant of pseudo-first-order equation (min^{-1}) and $k_{2,ads}$ is the biosorption constant of pseudo-second-order equation (min^{-1} g biosorbent mg^{-1} MB).

Both models fit well the experimental data for the three biosorbents in the range of MB concentrations studied (Fig. 10(a and b)). Model parameters and statistical parameters are presented in Tables 6 and 7. Model performances were compared using an *F*-test, and results show that, although the pseudo-second-order model is better for the majority of the experiments, no significant difference exists between the two models when considering the whole set of experiments.

However, when just comparing the experimental and predicted equilibrium uptake capacities (Tables 6 and 7), the pseudo-first-order model seems to be better.

The initial biosorption rate ($r_{ads}(i)$) can be calculated from:

$$\left.\frac{dq}{dt}\right|_{t=0} = r_{ads}(i) \quad (20)$$

So,

$$r_{ads}(i) = k_{1,ads} q_{eq} \quad (21)$$

and

$$r_{ads}(i) = k_{2,ads} q_{eq}^2 \quad (22)$$

for the pseudo-first-order (Eq. (21)) and pseudo-second-order models (Eq. (22)), respectively.

Increasing the initial MB concentration, the equilibrium uptake capacity and the initial adsorption rate increases, and the kinetic constants for both models are lower (Tables 6 and 7). As the initial MB concentration increases, the driving force between the liquid and solid phase increases, then decreasing the diffusion time of MB molecules from solution to the binding sites. The initial biosorption rate increases in the following order: algae *Gelidium* < composite material < algal waste. During the agar extraction process from algae *Gelidium*, using high NaOH concentrations, the porosity of the algae particles increases, which allows a faster diffusion of the MB molecules. As the active component of the composite material is the algal waste, the only difference between algal waste and the composite material is the resistance to diffusion due the thin layer of PAN.

4. Conclusions

The biosorbent particles selected for this work were characterized in terms of size distribution by using the Coulter Counter, scanning electron microscopy and image analysis techniques.

Real density was determined by helium picnometry and apparent density and distribution of macro and mesopores by mercury porosimetry.

Specific surface area was evaluated by dry (N_2 adsorption) and wet (methylene blue adsorption) methods. The wet method reflects better the real surface area available for metal adsorption because it is based on adsorption from solution. However, the assumption of covered area can affect the estimation of specific surface by more than 100%.

Methylene blue is well removed from aqueous solutions by the three biosorbents, when compared with other adsorbents, such as the traditional activated carbon.

Adsorption kinetics is well described by the pseudo-first order and pseudo-second order models. Increasing the initial MB concentration, equilibrium uptake capacity and initial adsorption rates increases.

Acknowledgements

Financial support by FCT and European community through FEDER (project POCI/AMB/57616/2004) is gratefully acknowledged. The authors are grateful to FCT for V. Vilar's doctorate scholarship.

References

[1] K.-C. Chen, J.-Y. Wua, C.-C. Huang, Y.-M. Liang, S.-C.J. Hwang, Decolorization of azo dye using PVA-immobilized microorganisms, J. Biotechnol. 101 (2003) 241–252.
[2] R. Gong, M. Li, C. Yang, Y. Sun, J. Chen, Removal of cationic dyes from aqueous solution by adsorption on peanut hull, J. Hazard. Mater. B121 (2005) 247–250.
[3] V. Vadivelan, K.V. Kumar, Equilibrium, kinetics, mechanism, and process design for the sorption of methylene blue onto rice husk, J. Colloid Interface Sci. 286 (2005) 90–100.
[4] S.S. Barton, The adsorption of methylene blue by active carbon, Carbon 25 (1987) 343–350.
[5] N. Kannan, M.M. Sundaram, Kinetics and mechanism of removal of methylene blue by adsorption on various carbons—a comparative study, Dyes Pigments 51 (2001) 25–40.
[6] G.P. Handreck, T.D. Smith, Adsorption of methylene blue from aqueous solutions by ZSM-5-type zeolites and related silica polymorphs, J. Chem. Soc. Faraday Trans. 84 (1988) 4194–4201.
[7] A. Gürses, S. Karaca, Ç. Dogar, R. Bayrak, M. Açikyildiz, M. Yalçin, Determination of adsorptive properties of clay/water system: methylene blue sorption, J. Colloid Interface Sci. 269 (2004) 310–314.
[8] S. Tanada, T. Kita, K. Boki, Mechanism of adsorption of methylene blue on magnesium silicate, Chem. Pharm. Bull. 28 (1980) 2503–2506.
[9] K.S. Low, C.K. Lee, K.K. Tan, Biosorption of basic dyes by water *Hyacinth* roots, Biores. Technol. 52 (1995) 79–83.
[10] C.-K. Lee, K.-S. Low, L.-C. Chung, Removal of some organic dyes by hexane-extracted spent bleaching earth, J. Chem. Technol. Biotechnol. 69 (1997) 93–99.
[11] F. Banat, S. Al-Asheh, L. Al-Makhadmeh, Evaluation of the use of raw and activated date pits as potential adsorbents for dye containig waters, Proc. Biochem. 39 (2003) 193–202.
[12] I.A. Rahman, B. Saad, Utilization of guava seeds as a source of activated carbon for removal of methylene blue from aqueous solution, Malaysian J. Chem. 5 (2003) 008–014.
[13] M. Dogan, M. Alkan, Y. Onganer, Adsorption of methylene blue from aqueous solution onto perlite, Water Air Soil Pollut. 120 (2000) 229–248.
[14] E. Rubin, P. Rodriguez, R. Herrero, J. Cremades, I. Barbara, M.E.S.d. Vicente, Removal of methylene blue from aqueous solutions using as biosorbent *Sargassum muticum*: an invasive macroalga in Europe, J. Chem. Tech. Biotechnol. 80 (2005) 291–298.
[15] V.J.P. Vilar, C.M.S. Botelho, R.A.R. Boaventura, Influence of pH, ionic strength and temperature on lead biosorption by *Gelidium* and agar extraction algal waste, Proc. Biochem. 40 (2005) 3267–3275.
[16] V.J.P. Vilar, F. Sebesta, C.M.S. Botelho, R.A.R. Boaventura, Equilibrium and kinetic modelling of Pb^{2+} biosorption by granulated agar extraction algal waste, Proc. Biochem. 40 (2005) 3276–3284.
[17] S.-Y. Mak, D.-H. Chen, Fast adsorption of methylene blue on polyacrylic acid-bound iron oxide magnetic nanoparticles, Dyes Pigments 61 (2004) 93–98.
[18] C.H. Giles, A.P.D. Silva, Molecular sieve effects of powder towards dues. Measurement of porosity by dye adsorption, Trans. Faraday Soc. 65 (1969) 1943–1951.
[19] S. Brunauer, P.H. Emmett, E. Teller, Adsorption of gases in multimolecular layers, J. Am. Chem. Soc. 60 (1938) 309–319.
[20] K. Bergmann, C.T. O'Konski, A spectroscopic study of methylene blue monomer, dimmer, and complexes with montmorillonite, J. Phys. Chem. 67 (1963) 2169–2177.
[21] S.J. Gregg, K.S.W. Sing, Adsorption, Surface Area and Porosity, Academic Press, New York, 1982.
[22] V.L.G. Mata, Caracterização de meios porosos. Porosimetria. Modelização 3D e tomografia seriada. Aplicação a suportes catalíticos, Ph.D. Thesis, Faculdade de Engenharia da Universidade do Porto, Porto, Portugal, 1998.
[23] P. Waranusantigul, P. Pokethitiyook, M. Kruatrachue, E.S. Upatham, Kinetics of basic dye (methylene blue) biosorption by giant duckweed (*Spirodela polyrrhiza*), Environ. Pollut. 125 (2003) 385–392.
[24] I. Langmuir, The adsorption of gases on plane surfaces of glass, mica and platinum, J. Am. Chem. Soc. 40 (1918) 1361–1403.
[25] R. Sips, On the structure of a catalyst surface, J. Chem. Phys. 16 (1948) 490–495.
[26] V.J.P. Vilar, Remoção de iões metálicos em solução aquosa por resíduos da indústria de extracção do agar, Ph.D. Thesis, Faculdade de Engenharia da Universidade do Porto, Porto, 2006.
[27] K. Imamura, E. Ikeda, T. Nagayasu, T. Sakiyama, K. Nakanishi, Adsorption behavior of methylene blue and its congeners on a stainless steel surface, J. Colloid Interface Sci. 245 (2002) 50–57.
[28] P.T. Hang, G.W. Brindley, Methylene blue adsorption by clay minerals: determination of surface areas and cation exchange capacities (clay-organic studies XVIII), Clays Clay Miner. 18 (1970) 203–212.

[29] R. Aringhieri, G. Pardini, M. Gispert, A. Solé, Testing a simple methylene blue method for surface area estimation in soils, Agrochimica 36 (1992) 224–232.
[30] G. Chen, J. Pan, B. Han, H. Yan, Adsorption of methylene blue on montmorillonite, J. Dispersion Sci. Technol. 20 (1999) 1179–1187.
[31] G. Hähner, A. Marti, N.D. Spencer, W.R. Caseri, Orientation and electronic structure of methylene blue on mica: a near edge X-ray adsorption fine structure spectroscopy study, J. Chem. Phys. 104 (1996) 7749–7757.
[32] M. Borkovec, M. Wu, G. Degovics, P. Laggner, H. Sticher, Surface area and size distributions of soil particles, Colloids Surf. A 73 (1993) 65–76.
[33] K.S.W. Sing, D.H. Everett, R.A.W. Hauk, L. Moscou, R.A. Pierotti, J. Rouquerol, T. Siemienieweska, Reporting physisorption data for gas/solid systems with special reference to the determination of surface-area and porosity, Pure Appl. Chem. 57 (1985) 603–619.
[34] D. DeVault, The theory of chromatography, J. Am. Chem. Soc. 65 (1943) 532–540.
[35] F. Rouquerol, J. Rouquerol, K. Sing, Adsorption by Powders and Porous Solids, Academic Press, London, 1999.
[36] S.J. Gregg, K.S.W. Sing, Adsorption, Surface Area and Porosity, Academic Press, London, 1991.
[37] J.C. Echeverria, M.T. Morera, C. Mazquiaran, J.J. Garrido, Characterization of the porous structure of soils: Adsorption of nitrogen (77 K) and carbon dioxide (273 K), and mercury porosimetry, Eur. J. Soil Sci. 50 (1999) 497–503.
[38] J.C. Santamarina, K.A. Klein, Y.H. Wang, E. Prencke, Specific surface: determination and relevance, Can. Geotech. J. 39 (2002) 233–241.
[39] L.M. HE, B.M. Tebo, Surface charge properties of and Cu(II) adsorption by spores of the marine *Bacillus* sp. Strain sg-1, Appl. Environ. Microbiol. 64 (1998) 1123–1129.
[40] C. Kaewprasit, E. Hequet, N. Abidi, J.P. Gourlot, Application of methylene blue adsorption to cotton fiber specific area measurement. Part I. Methodology, J. Cotton Sci. 2 (1998) 164–173.
[41] V.J.P. Vilar, C.M.S. Botelho, R.A.R. Boaventura, Equilibrium and kinetic modelling of Cd(II) biosorption by algae *Gelidium* and agar extraction algal waste, Water Res. 40 (2006) 291–302.
[42] G. McKay, G. Ramprasad, P. Pratapamowli, Equilibrium studies for the adsorption of dyestuffs from aqueous solution by low-cost materials, Water Air Soil Pollut. 29 (1986) 273–283.
[43] K.S. Low, C.K. Lee, L.L. Heng, Sorption of basic dyes by *Hydrilla verticillata*, Environ. Technol. 15 (1994) 115–124.